Biosensors and Bioelectronics 166 (2020) 112424

Contents lists available at ScienceDirect

Biosensors and Bioelectronics

journal homepage: http://www.elsevier.com/locate/bios

Ultrasensitive colorimetric biosensor for BRCA1 mutation based on multiple signal amplification strategy

Yunfei Bai [a], Huizhen Li [a], Jun Xu [b], Yufan Huang [c], Xiuming Zhang [a], Jian Weng [a,**], Zhu Li [d,***], Liping Sun [a,*]

[a] Key Laboratory of Biomedical Engineering of Fujian Province, Department of Biomaterials, College of Materials, Xiamen University, Xiamen, 361005, China
[b] Department of Physics, Research Institute for Biomimetics and Soft Matter, Fujian Provincial Key Laboratory for Soft Functional Materials, Xiamen University, Xiamen, 361005, China
[c] Department of Breast Surgery, The First Affiliated Hospital of Xiamen University, Xiamen, 361003, China
[d] Xiamen Nuokangde Biological Technology Co., Ltd, Xiamen, 361006, China

ARTICLE INFO

Keywords:
Colorimetric biosensor
Signal amplification
BRCA1
2D nanomaterials
Gold nanoparticles
Bismuth selenide nanosheets

ABSTRACT

Colorimetric biosensors have attracted wide attention due to their low cost, simple operation, rapid response and good reproducibility. However, insufficient sensitivity limits their applications. This report describes the design of a colorimetric biosensor based on a three-step multiple signal amplification strategy to detect breast cancer-associated BRCA1 mutation. The capture unit, signal unit, and target DNA form a sandwich construction. The signal probes are immobilized on the surface of nanomaterials to form the signal unit, which can catalyze the reduction of a colorimetric substrate 4-nitrophenol (4-NP). Firstly, 0D gold nanoparticles (AuNPs) are employed to catalyze 4-NP reduction and reaches 10^2-fold signal amplification. Then AuNPs are decorated on the surface of 2D material, such as graphene oxide (GO), the catalytic efficiency is further enhanced to 10^4-fold signal amplification. The third step amplification is achieved by replacing stable GO with oxidizable 2D material (Bi_2Se_3 nanosheets), resulting in a nearly 10^{10}-fold amplification. The sandwich-type Bi_2Se_3-AuNPs biosensor shows excellent sensitivity and selectivity. The detection limit can reach up to 10^{-18} M and there is a good linear relationship between the reaction kinetics constant and the DNA concentration in the range of 10^{-12}-10^{-18} M. In addition, one-base mismatch, two-base mismatch and non-complementary sequences can be distinguished clearly by this biosensor. This design may have beneficial clinical application prospects for cancer genetic screening and early diagnosis.

1. Introduction

According to the report of International Agency for Research on Cancer, breast cancer remains a worldwide health threat to women. It is the most frequently diagnosed cancer (24.2%) and the leading cause of cancer death among females (15.0%) (Bray et al., 2018). Most current cancer patients are diagnosed when the tumor is already formed or at an even late stage. Cancer-related genetic biomarkers can be detected during the early stages of cancer or even before the cancer cell is formed. Thus, nucleic acid analysis can assist in more precise screening and early diagnosis of cancer. Different strategies have been developed, such as colorimetric, fluorescence, chemiluminescence, and electrochemical biosensors (Bray et al., 2018; Peng et al., 2017; Chen et al., 2016; He et al., 2012; Al-Ogaidi et al., 2014; Fayazfar et al., 2014). Colorimetric analysis has attracted much attention due to its convenience, low cost, quick feedback and good reproducibility (Bray et al., 2018). Colorimetric assays have been widely used in the field of clinical diagnosis, such as detection of nucleic acids, protein biomarkers, infectious microorganisms, viruses and metal ions (Vigneshvar et al., 2016; Xiao et al., 2017). However, insufficient sensitivity limits its application.

In order to obtain lower detection limit, different strategies have been developed to amplify the colorimetric signal. Nanomaterials, such as zero-dimensional nanoparticles (gold, silver, copper), one-dimensional nanomaterials (carbon nanotubes, silicon nanowire,

* Corresponding author.
** Corresponding author.
*** Corresponding author.
E-mail addresses: jweng@xmu.edu.cn (J. Weng), lizhu@nkdbio.com (Z. Li), sunliping@xmu.edu.cn (L. Sun).

https://doi.org/10.1016/j.bios.2020.112424
Received 22 April 2020; Received in revised form 15 June 2020; Accepted 2 July 2020
Available online 11 July 2020

nickel telluride nanowires), two-dimensional nanomaterials (graphene, few-layer black phosphorus, hexagonal boron nitride, Bi_2Se_3 nanosheets), etc. have been reported to improve the sensitivity of colorimetric DNA biosensors based on either aggregation of gold nanoparticles (AuNPs) or the peroxidase-like activity of nanomaterials. Combined with DNA amplification technology, the sensitivity can be further improved. The limit of colorimetric detection of DNA is between nM-fM level (Table S1). The combination of nanomaterials (nanocomposites) appears to be a promising approach to improve the efficiency of the colorimetric biosensors. For example, Au/Pt nanocluster and graphene-AuNPs hybrids have been used for DNA analysis with a detection limit of pM level (Dehghani et al., 2019; Chen et al., 2016). In our study, a multiple-signal amplification strategy is developed to enhance the sensitivity of DNA biosensor. The sensitivity of this colorimetric sensor is dramatically improved by three-step signal amplifications, resulting in a nearly 10^{10}-fold amplification. Up to 10^{-18} M target DNA carrying breast cancer-associated mutation can be detected. Our research provides a new tool for simple and quick screening of breast cancer by multiple-signal amplification strategy.

2. Materials and methods

2.1. Preparation of AuNPs and 2D nanomaterial-AuNPs composites

AuNPs, graphene oxide (GO), and Bi_2Se_3 nanosheets were prepared according to previous methods (Supporting information 2.1). GO-AuNPs and Bi_2Se_3-AuNPs nanocomposites were synthesized by in situ reduction of $HAuCl_4$ on 2D nanomaterials surface (Supporting information 2.2).

2.2. Construction of colorimetric biosensor for BRCA1 mutation detection

Gold film was sputtered on 0.5 × 0.5 cm silicon wafer by ion beam sputter deposition. Gold-coated silicon wafer was immersed in 3′ thiolated capture probes (1 pM) for 30 min, then the wafer was washed with water to remove unbound capture probes. 20 μL of 0.1 mg mL^{-1} Bi_2Se_3-AuNPs was mixed with 5' thiolated signal probes (10 fM) thoroughly, and the unbound probes were removed by centrifugation at 12000 rpm for 10 min. The capture probe-modified silicon wafer was incubated with the target BRCA1 DNA for 30 min, rinsed with water, then incubated with the signal probe-modified Bi_2Se_3-AuNPs (0.1 mg mL^{-1}) for 30 min, rinsed with water to remove unbound Bi_2Se_3-AuNPs, forming a sandwich structure, as shown in Fig. 1a. The sandwich structure was placed in fresh 4-NP/$NaBH_4$ solution and measured with UV-vis spectrophotometer. AuNPs and GO-AuNPs biosensors were constructed in similar methods as Bi_2Se_3-AuNPs biosensor.

3. Results and discussions

3.1. Detection principle

Single-stranded DNA (ssDNA) carrying a BRCA1 nonsense mutation (3607C > T, supporting information) was selected as the target DNA according to an investigation of the prevalence of BRCA mutations in Chinese patients with breast-ovarian cancer (Sung et al., 2017). The colorimetric sandwich-type biosensor consists of a signal unit and a capture unit (Fig. 1a). The signal probes are first immobilized on the surface of Bi_2Se_3-AuNPs via Au-S bonds to form the signal unit. Then the capture probes are attached on the gold-coated silicon wafer to obtain the capture unit, which could capture one end of target DNA by complementary pairing. Finally, the signal unit hybridize with the other end of the target DNA to create a sandwich construction. Bi_2Se_3-AuNPs catalyze the reduction of 4-NP to 4-aminophenol (4-AP) for colorimetric assay.

3.2. Performance of the colorimetric biosensor

The colorimetric biosensor is based on the catalytic activity for the reduction of a colorimetric substrate 4-NP to 4-AP. The color of 4-NP/$NaBH_4$ solution turned from bright yellow to colorless (Fig. 1b, insert), confirming the catalytic activity of AuNPs and 2D nanomaterial-AuNPs composites. Time-dependent UV-vis spectra showed that the peak at 400 nm disappeared, whereas a new peak at 300 nm appeared gradually, which is a characteristic absorption of the reduction product 4-AP (Fig. 1b) (Choi et al., 2014). There is a linear correlation between ln A/A_0 (A_0 is the original absorbance intensity of 4-NP at 400 nm, while A is the final absorbance intensity at 400 nm after reduction by Bi_2Se_3-AuNPs) and reduction time (Fig. S3). The first-order reaction rate constant k is obtained from the slope of the straight line plotting by ln A/A_0 against time. The reaction cannot proceed without catalyst or with Bi_2Se_3 (Fig. S3, black line and red line). AuNPs demonstrated less catalytic activity ($k = 3.13 \times 10^{-4}$ S^{-1}) than the Bi_2Se_3-AuNPs nanocomposite ($k = 1.26 \times 10^{-3}$ S^{-1}). A simple mixing of Bi_2Se_3 nanosheets with AuNPs exhibited poorer catalytic performance than the Bi_2Se_3-AuNPs nanocomposite, indicating that the interaction between AuNPs and Bi_2Se_3 nanosheets was necessary to achieve synergetic effect on catalytic performance. This result proved that Bi_2Se_3-AuNPs nanocomposite had superior catalytic performance than AuNPs and GO-AuNPs, which was in accordance with previous report (Xiao et al., 2017).

Due to the limitation of the colorimetric method based on Lambert Beer's law, the minimum concentration of detectable solution is 10^{-8} M (Demertzis, 2004). We investigated the sensing performance of AuNPs, GO-AuNPs and Bi_2Se_3-AuNPs biosensors for BRCA1 gene detection and found that the sensitivity of the colorimetric biosensor was improved step by step. Firstly, 0D AuNPs were used to construct the sandwich-type colorimetric biosensor. The detection limit for BRCA1 was up to 10^{-10} M (100 pM, Fig. S1c), which reached 10^2-fold signal amplification. Then AuNPs were decorated on the surface of 2D GO to construct the GO-AuNPs biosensor, which improved the detection limit to 10^{-12} M (1 pM, Fig. S1d) and the signal was further amplified 10^4 times. The third step amplification was achieved by replacing stable GO with oxidizable 2D material (Bi_2Se_3 nanosheets) and loading equivalent amount of AuNPs (Fig. S4). The detection limit reached 10^{-18} M (1 aM, Fig. 1c), resulting in a nearly 10^{10}-fold signal amplification. The reaction rate constants of samples without Bi_2Se_3-AuNPs or without target DNA were almost the same (6.53×10^{-5} S^{-1} and 7.72×10^{-5} S^{-1}), indicating no reduction of 4-NP. The target DNA serves as a bridge between capture unit and signal unit. In the absence of target DNA, the sandwich structure cannot be formed, thus Bi_2Se_3-AuNPs nanocomposite cannot be connected with the silicon wafer to catalyze the colorimetric reaction. There was a good linear relationship between k and the concentrations of target DNA in a wide range of 10^{-18} M-10^{-12} M ($R^2 = 0.99$) (Fig. 1d). The detection limit of Bi_2Se_3-AuNPs biosensor was much lower than other colorimetric DNA biosensors using 0D, 1D, 2D or hybrid nanomaterials (Table S1).

In order to investigate the selectivity of Bi_2Se_3-AuNPs biosensor, one-base mismatch, two-base mismatch and non-complementary sequences were designed. Three parallel experiments were set, in which the concentrations of the complete complementary sequences were 1 pM, 10 pM, and 100 pM respectively. The concentration of the interference sequences (mismatched and non-complementary DNA) in the control group was 10^3 times larger than the experimental group (complementary DNA). Even though the concentration of the control group was much higher than that of the experimental group, k values of the mismatched and non-complementary DNA were much lower than that of the complementary DNA. One-base mismatch, two-base mismatch and non-complementary sequences could be distinguished clearly (Fig. 1e). These results confirmed the ultrasensitive performance and high selectivity of Bi_2Se_3-AuNPs biosensor.

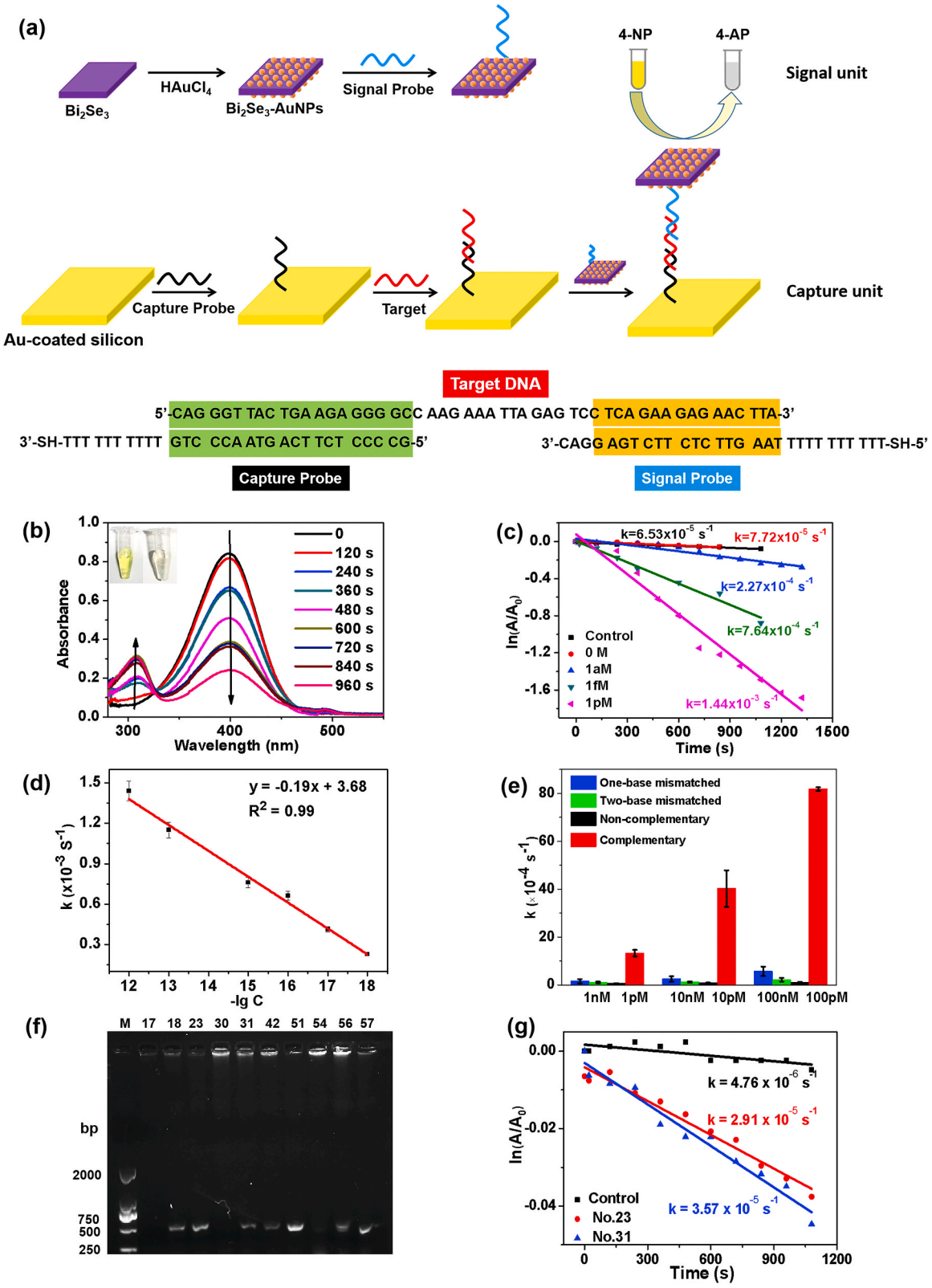

Fig. 1. (a) The detection principle of the colorimetric sandwich-type biosensor. (b) UV-vis absorption spectrum of 4-NP reduced by Bi_2Se_3-AuNPs. Inset: 4-NP before and after reaction. (c) Detection of BRCA1 mutation using Au/Bi_2Se_3 colorimetric biosensor. The target DNA concentrations were 0 M, 1 pM, 1 fM, and 1 aM, respectively. 100 μL of target DNA was added. No signal probe-modified Au/Bi_2Se_3 was added in the control sample. (d) Relationship between the reaction rate constant k and target DNA concentration. (e) Selectivity of the colorimetric biosensor at different target DNA concentrations. K values of one-base mismatched (blue), two-base mismatched (green), non-complementary (black) and complementary sequences (red) were compared. (f) Agarose electrophoresis of genomic DNA extracted from clinical samples. (g) Reaction kinetic constant of PCR products containing BRCA1 mutations (red and blue). Control: Sample containing no BRCA1 mutation (black). (For interpretation of the references to color in this figure legend, the reader is referred to the Web version of this article.)

3.3. Mechanism of the colorimetric biosensor and signal amplification

In order to confirm that the signal probes were bound to Bi_2Se_3-AuNPs nanocomposite, FAM-modified signal probes were incubated with Bi_2Se_3-AuNPs and centrifuged to remove unbound signal probes. The fluorescence intensity of the supernatant was significantly lower than that of the FAM-modified signal probes, indicating that part of the thiol-modified probes were bound to Bi_2Se_3-AuNPs by Au-S bond (Fig. 2a). The precipitate (signal probe-modified Bi_2Se_3-AuNPs) showed no fluorescence since FAM was quenched by the nanocomposite.

Fluorescent spots study was performed to investigate the interaction between target DNA and capture probes. SYBR green I was used to dye the complementary double-stranded DNA (dsDNA) (Dragan et al., 2012). When no target DNA or non-complementary sequence reacted with the capture probes, there was no fluorescent signal present. In the presence of high-concentration one-base mismatched DNA (1 μM), weak fluorescent spots appeared, indicating partial formation of dsDNA. The fluorescence intensity increased with increasing concentration of complementary target sequences, confirming more dsDNA formed at higher target DNA amount (Fig. 2b).

In order to visualize the sandwich structure of the biosensor, the silicon wafer was replaced by a gold-coated glass slide modified with capture probes, then connected to the signal probe-modified Bi_2Se_3-AuNPs nanocomposite by target DNA. At high concentration of completely non-complementary and one-base mismatched target DNA (10 μM), there was no fluorescence in the dark field. When complementary target sequences were added, green fluorescence can be observed in the dark field even at very low concentration (10 pM, Fig. 2c). With the increase of the complementary target DNA concentration, the fluorescence distribution area increased in the dark field, since more dsDNA were formed. Meanwhile, the amount of nanosheets in the bright field also increased. Merge of the bright and dark field images showed that the nanosheets overlapped with the fluorescence, indicating successful construction of the sandwich-type biosensor.

Our colorimetric biosensor is based on a three-step signal amplification strategy (Fig. 3a). The first step signal amplification is realized by gold nanoparticles catalysis. The two-dimensional substrate (such as GO and Bi_2Se_3 nanosheet) provides a platform for AuNPs to distribute on their surface uniformly and prevent aggregation of AuNPs, thus increasing their stability and catalytic efficiency. Compare with stable GO, Bi_2Se_3 as a topological insulator is more likely to be oxidized and lose electrons. As an effective conductor of electrons, AuNPs loaded on the surface of Bi_2Se_3 nanosheets can transfer the enriched electrons, further accelerate 4-NP reduction and amplify the signal significantly. Zeta potential measurements showed that after catalyzing 4-NP reaction, the potential of Bi_2Se_3-AuNPs shifted from 2.0 ± 0.4 mV to -2.5 ± 0.7 mV, indicating loss of electrons in the Bi_2Se_3 oxidation process (Fig. 3b). XPS data revealed that compared with Bi_2Se_3, Se in Bi_2Se_3-AuNPs was partially oxidized and the characteristic peak of selenium oxide at 58.8 ev indicated that Bi_2Se_3 reacted with $HAuCl_4$. After catalyzing 4-NP, the SeO_x peak increased and the Se peak decreased, indicating that part of Se in Bi_2Se_3 lost electrons and produced selenium oxide (SeO_x) (Fig. 3c).

To further explore the electron donor property of Bi_2Se_3, polydopamine (PDA) was coated onto AuNPs and Bi_2Se_3 to block electron transfer. Dopamine was stirred with AuNPs and Bi_2Se_3 for 0.5 h, 3 h, and 24 h, respectively to obtain materials with different thickness of PDA (Lee et al., 2007). Then PDA-covered Bi_2Se_3 reacted with $HAuCl_4$ to yield Bi_2Se_3-PDA-AuNPs. At 0.5 h reaction time, only a part of AuNPs were covered by PDA, therefore AuNPs still remained their catalytic activity ($k = 8.44 \times 10^{-4}\ S^{-1}$, Fig. 3d). When AuNPs were totally covered by PDA after 24 h reaction, PDA inhibited the catalytic activity of AuNPs and hindered 4-NP reduction ($k = 2.97 \times 10^{-5}\ S^{-1}$). For Bi_2Se_3-PDA-AuNPs, Bi_2Se_3 was isolated by PDA from AuNPs. With the increase of film thickness (Fig. S6), the catalytic effect decreased significantly, which was finally comparable to that of AuNPs ($k = 2.90 \times 10^{-4}\ S^{-1}$, Fig. 3e). These results proved that blocking electron transport can inhibit the catalytic efficiency of Bi_2Se_3-AuNPs, indicating

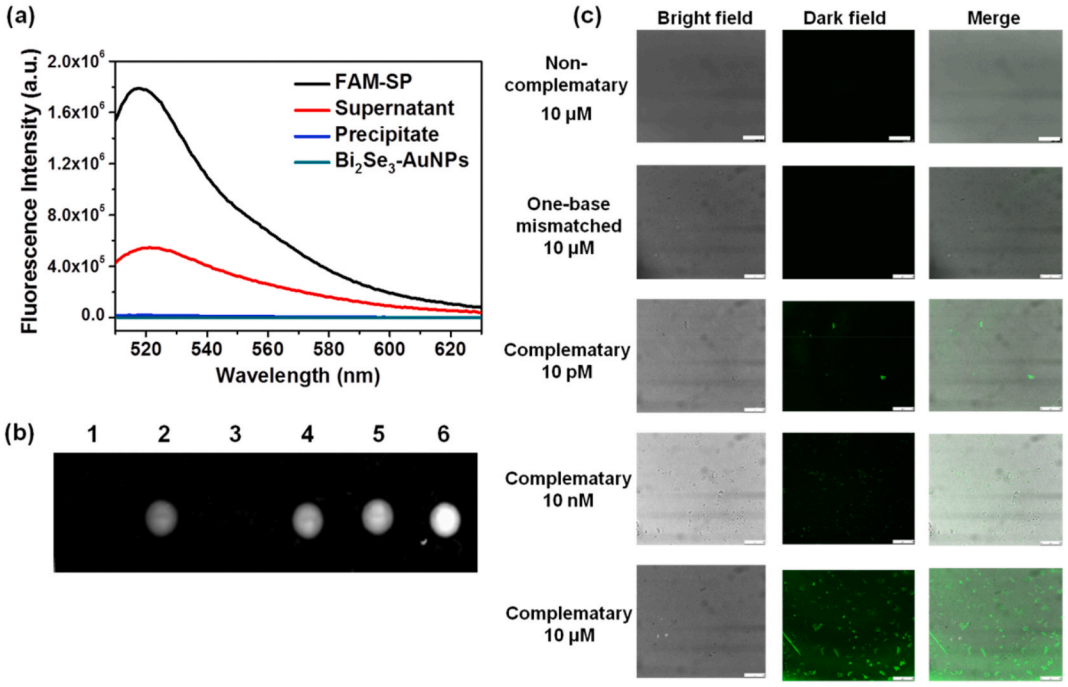

Fig. 2. Mechanism of the colorimetric sandwich-type biosensor. (a) Fluorescence spectra of FAM-modified signal probe (FAM-SP, black), supernatant (red), precipitate (FAM-SP modified Bi_2Se_3-AuNPs, blue), Bi_2Se_3-AuNPs (green). (b) Fluorescence spots of capture probes hybridized with target sequences. 1. No target DNA, 2. one-base mismatched DNA (1 μM), 3. non-complementary DNA (1 μM), 4. Complementary DNA (0.1 nM), 5. Complementary DNA (10 nM), 6. Complementary DNA (1 μM). (c) Images of laser scanning confocal microscope of the sandwich-type biosensor (the scale is 25 μm). SYBR Green was used to dye hybridized dsDNA. (For interpretation of the references to color in this figure legend, the reader is referred to the Web version of this article.)

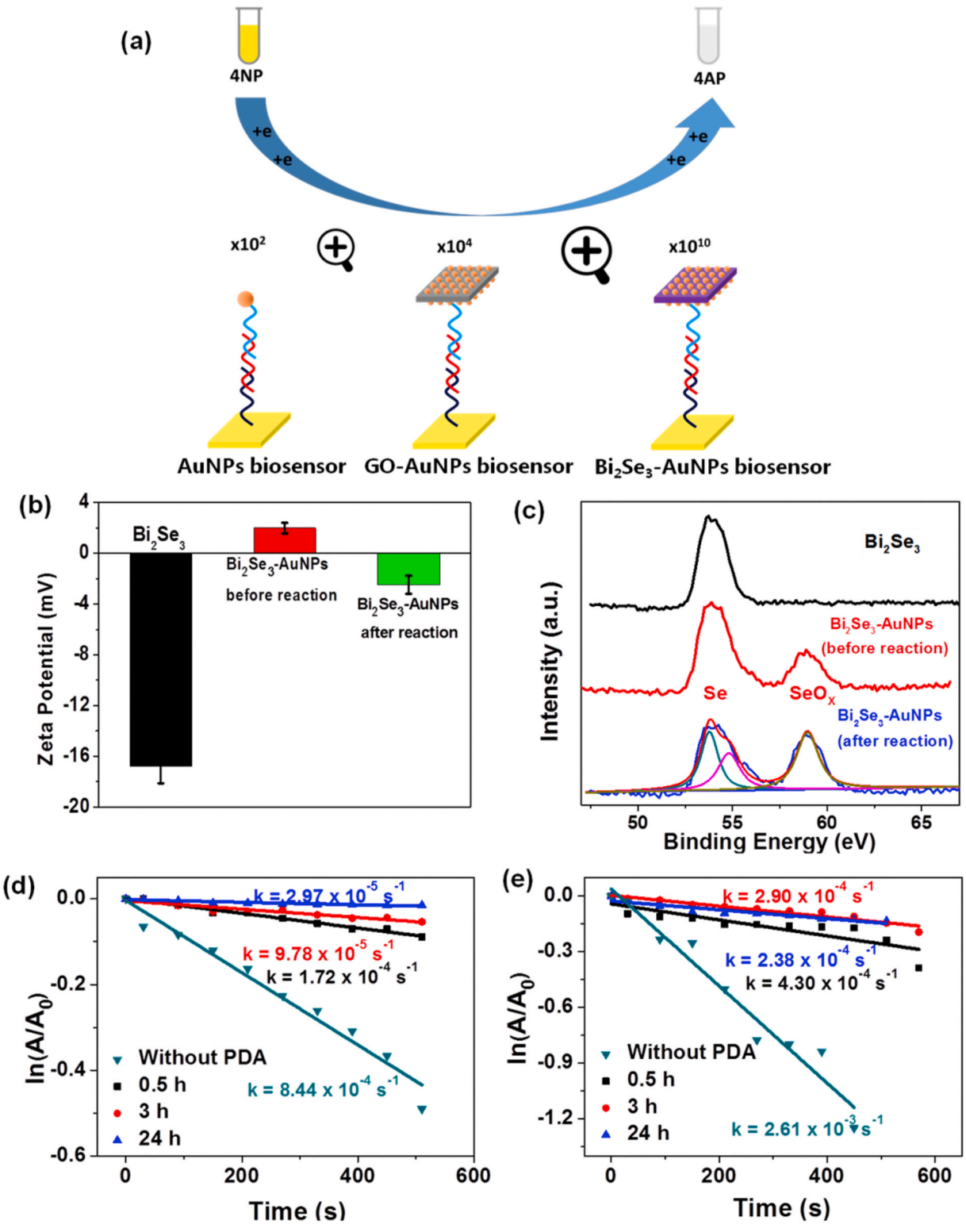

Fig. 3. Mechanism of the signal amplification. (a) Multiple-signal amplification of the colorimetric biosensor. (b) Zeta potentials of Bi_2Se_3 (black), Bi_2Se_3-AuNPs before (red) and after (green) catalyzing 4-NP reduction. (c) XPS spectra of Bi_2Se_3 (black), Bi_2Se_3-AuNPs before (red) and after (blue) catalyzing 4-NP reduction. (d) Plot of $\ln(A/A_0)$ versus time for 4-NP reduction by PDA-coated AuNPs. Dopamine was stirred with AuNPs for 0.5 h, 3 h, and 24 h to obtain PDA-coated AuNPs with different thickness of PDA. (e) Plot of $\ln(A/A_0)$ versus time for the reduction of 4-NP by Bi_2Se_3-PDA-AuNPs. Dopamine was mixed with Bi_2Se_3 for 0.5 h, 3 h, and 24 h to obtain PDA-coated Bi_2Se_3 with different thickness of PDA. (For interpretation of the references to color in this figure legend, the reader is referred to the Web version of this article.)

the role of Bi_2Se_3 as electron donor in 4-NP reduction reaction.

The oxidability of Bi_2Se_3-AuNPs is both the advantage and limitation of this biosensor. Oxidation of Bi_2Se_3 nanosheets can produce electrons for 4-NP reduction reaction. However, Bi_2Se_3-AuNPs nanocomposite should be freshly prepared to maintain its catalytic activity and the catalyst cannot be reused.

3.4. Detection of clinical samples

Genomic DNA extracted from the blood samples of breast cancer patients was amplified by PCR and analyzed by agarose gel electrophoresis (Fig. 1f). DNA sequencing confirmed that samples 23 and 31 contained a point mutation compared with control samples. New capture probe was designed complementary to the mutated region (Supporting information). Bi_2Se_3-AuNPs colorimetric biosensor was constructed to detect the PCR products of these two samples and the reaction kinetics constants were measured (Fig. 1g). The detection limits were 5.8 ng μL^{-1} and 3.2 ng μL^{-1}, respectively. K values of the PCR samples carrying mutation were 10-fold higher than that of the control PCR samples without mutation. Therefore, Bi_2Se_3-AuNPs colorimetric biosensor is capable of detecting clinical samples with good selectivity. The reaction rate constant of synthetic ssDNA target is higher (10^{-4} S^{-1} level, Fig. 1c) than PCR products (10^{-5} S^{-1} level, Fig. 1g), indicating lower performance of this biosensor for clinical samples. It could be due to following reasons: Firstly, synthetic ssDNA purified by high-performance liquid chromatography is highly pure. However, PCR products purified by silica-membrane-based column could still contain DNA primers, dNTP, DNA polymerase and other impurities, which might interfere the performance of this biosensor; Secondly, the DNA probes are more difficult to bind double-stranded PCR products than ssDNA, since part of hydrogen bonds need to be broken to expose the complementary region; Finally, the length of PCR fragments reaches 535 bp, while ssDNA target contains only 51 bases. Longer PCR fragments could be twisted to form tertiary structure, inhibiting the probes to recognize and bind the complementary sites. Further effort is required to improve the efficiency of the colorimetric biosensor for the detection of clinical samples.

4. Conclusion

Base on multiple-signal amplification strategy, a sandwich-type colorimetric biosensor was constructed to detect BRCA1 gene mutation of breast cancer. This biosensor exhibited excellent sensitivity and high selectivity with a detection limit of 10^{-18} M and a large dynamic range of 10^{-18} M - 10^{-12} M. In the future, such biosensor can be further modified with suitable molecular probes for potential application in detecting a broad range of other targets including virus RNA, proteins, exosomes, aptamer-binding small molecules, and cancer cells etc.

Declaration of competing interest

The authors declare that they have no known competing financial interests or personal relationships that could have appeared to influence the work reported in this paper.

CRediT authorship contribution statement

Yunfei Bai: Data curation, Writing - original draft. **Huizhen Li:** Visualization, Validation. **Jun Xu:** Resources. **Yufan Huang:** Resources. **Xiuming Zhang:** Project administration. **Jian Weng:** Conceptualization, Methodology. **Zhu Li:** Conceptualization, Methodology. **Liping Sun:** Conceptualization, Methodology, Funding acquisition, Supervision, Writing - review & editing.

Acknowledgement

This work was supported by the National Natural Science Foundation of China [81872415, 81571764]. We thank Ms. Alicia Burrus for editing this paper.

Appendix A. Supplementary data

Supplementary data to this article can be found online at https://doi.org/10.1016/j.bios.2020.112424.

References

Al-Ogaidi, I., Gou, H.L., Aguilar, Z.P., Guo, S.W., Melconian, A.K., Al-Kazaz, A.K.A., Meng, F.K., Wu, N.Q., 2014. Chem. Commun. 50 (11), 1344–1346.
Bray, F., Ferlay, J., Soerjomataram, I., Siegel, R.L., Torre, L.A., Jemal, A., 2018. CA Canc J Clin 68 (6), 394–424.
Chen, C., Li, N., Lan, J., Ji, X., He, Z., 2016. Anal. Chim. Acta 902, 154–159.
Choi, Y., Choi, M.J., Cha, S.H., Kim, Y.S., Cho, S., Park, Y., 2014. Nanoscale Res. Lett. 9 (1), 103.
Dehghani, Z., Hosseini, M., Mohammadnejad, J., Ganjali, M.R., 2019. Chemistry 4 (40), 11687–11692.
Demertzis, M.A., 2004. Anal. Chim. Acta 505 (1), 73–76.
Dragan, A.I., Pavlovic, R., McGivney, J.B., Casas-Finet, J.R., Bishop, E.S., Strouse, R.J., Schenerman, M.A., Geddes, C.D., 2012. J. Fluoresc. 22 (4), 1189.
Fayazfar, H., Afshar, A., Dolati, M., Dolati, A., 2014. Anal. Chim. Acta 836, 34–44.
He, Y., Lin, Y., Tang, H.W., Pang, D.W., 2012. Nanoscale 4 (6), 2054–2059.
Lee, H., Dellatore, S.M., Miller, W.M., Messersmith, P.B., 2007. Science 318 (5849), 426–430.
Peng, J., Lai, Y.Q., Chen, Y.Y., Xu, J., Sun, L.P., Weng, J., 2017. Small 13 (15), 1603589.
Sung, P.L., Wen, K.C., Chen, Y.J., Chao, T.C., Tsai, Y.F., Tseng, L.M., Qiu, J.T.T., Chao, K. C., Wu, H.H., Chuang, C.M., Wang, P.H., Huang, C.Y.F., 2017. PloS One 12 (9), e0185615.
Vigneshvar, S., Sudhakumari, C.C., Senthilkumaran, B., Prakash, H., 2016. Front. Bioeng. Biotechnol. 4, 11.
Xiao, L.P., Zhu, A.M., Xu, Q.C., Chen, Y., Xu, J., Weng, J., 2017. ACS Appl. Mater. Interfaces 9 (8), 6931–6940.